Cell Reports, Volume *39*

Supplemental information

Dynamic interplay between thalamic activity and Cajal-Retzius cells regulates the wiring of cortical layer 1

Ioana Genescu, Mar Aníbal-Martínez, Vladimir Kouskoff, Nicolas Chenouard, Caroline Mailhes-Hamon, Hugues Cartonnet, Ludmilla Lokmane, Filippo M. Rijli, Guillermina López-Bendito, Frédéric Gambino, and Sonia Garel

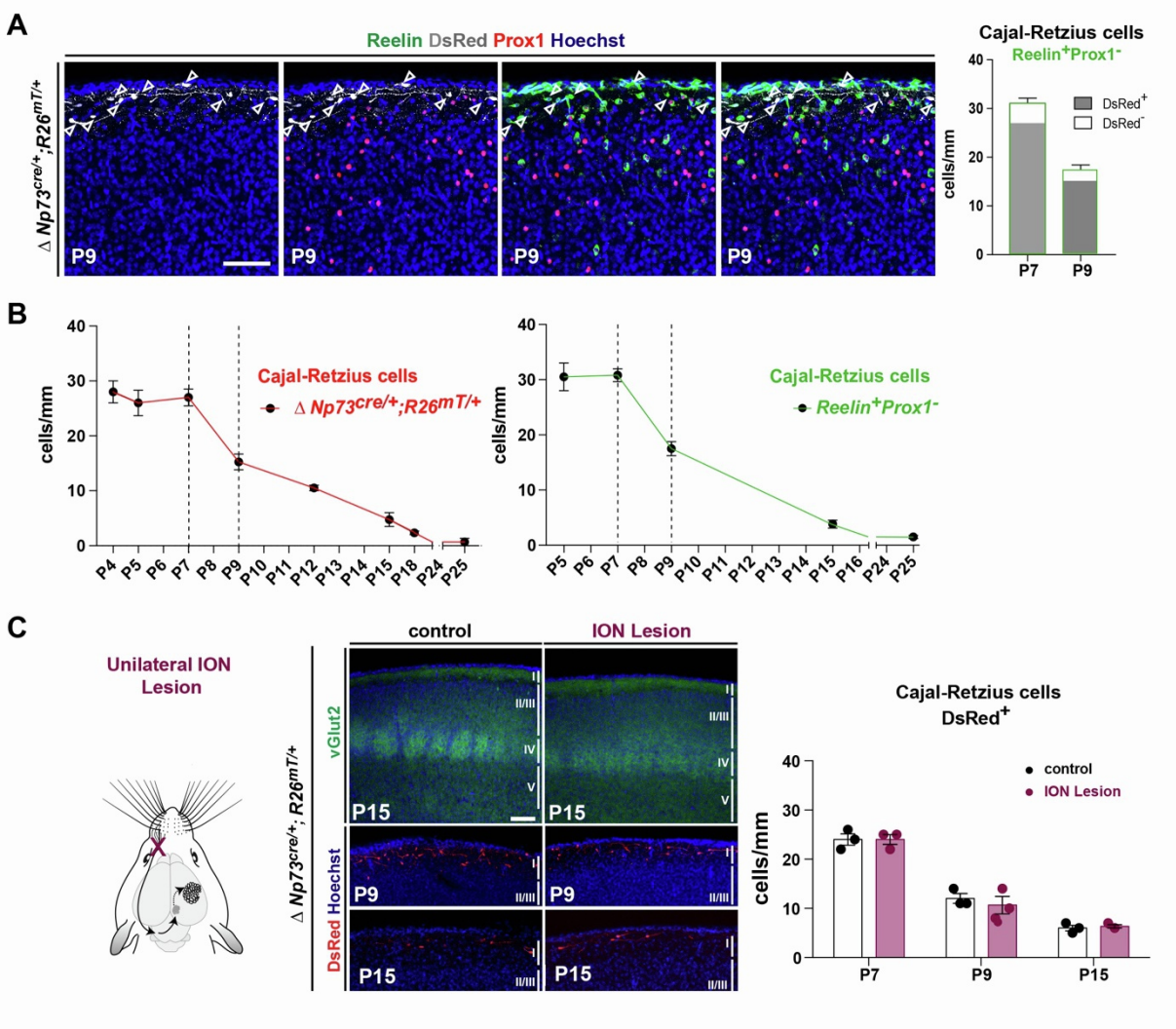

Figure S1, related to Figure 1. Different labelling strategies highlight Cajal-Retzius cell dynamics across development and sensory deprivation.

(A) Identification of Cajal-Retzius cells using the *ΔNp73*$^{cre/+}$*;R26*$^{mT/+}$ driver and co-immunostaining as Reelin^{+}Prox1^{-} cells at P9. Quantifications of the percentage of the *ΔNp73*$^{cre/+}$*;R26*$^{mT/+}$CRc out of the total number of CRc labelled with Reelin^{+}Prox1^{-} (right). At P7, 86.96% of the Reelin^{+}Prox1^{-} are DsRed^{+} in the *ΔNp73*$^{cre/+}$*;R26*$^{mT/+}$ line and at P9, 87.14% of the Reelin^{+}Prox1^{-} are DsRed^{+} in the *ΔNp73*$^{cre/+}$*;R26*$^{mT/+}$ line, consistently with previous reports (Ledonne et al., 2016; Tissir et al., 2009) showing that the *ΔNp73*$^{cre/+}$line targets approximatively 85% of CRc, as it does not label pallial-subpallial boundary-derived CRc (P7: n=22 for Reelin^{+}Prox1^{-} and n=6 for DsRed^{+}; P9: n=18 for Reelin^{+}Prox1^{-} and n=4 for DsRed^{+}). **(B)** Density of CRc (cells/mm length of L1) evaluated by genetic labeling (*ΔNp73*$^{cre/+}$) and by co-immunostaining (Reelin^{+}Prox1^{-}) at early postnatal stages reveal an acute period of elimination between P7 and P9 until their almost complete elimination in the somatosensory cortex by P25. (**C**) Schematic representation of a unilateral InfraOrbital Nerve (ION) lesion (left). Confocal images of sections across the barrel cortex (S1bf) of *ΔNp73*$^{cre/+}$*;R26*$^{mT/+}$ at P7, P9 and P15 in control and ION lesioned pups immunostained for DsRed (red) to label CRc. At P15, vGlut2 immunostaining reveals the lack of visible barrels in ION lesioned pups (middle). Quantification of CRc density (cells/mm of L1 length) shows no differences in controls and ION-lesioned pups (P7: n=3 controls, n=3 ION; P9: n=3 controls and n=3 ION, P15: n=3 controls and n=3 ION) (right). Values are expressed as mean ± SEM, 2-ways ANOVA test with Sidak's multiple comparison correction, *p < 0.05, **p< 0.01, ***p < 0.001. Scale bar represents 100µm.

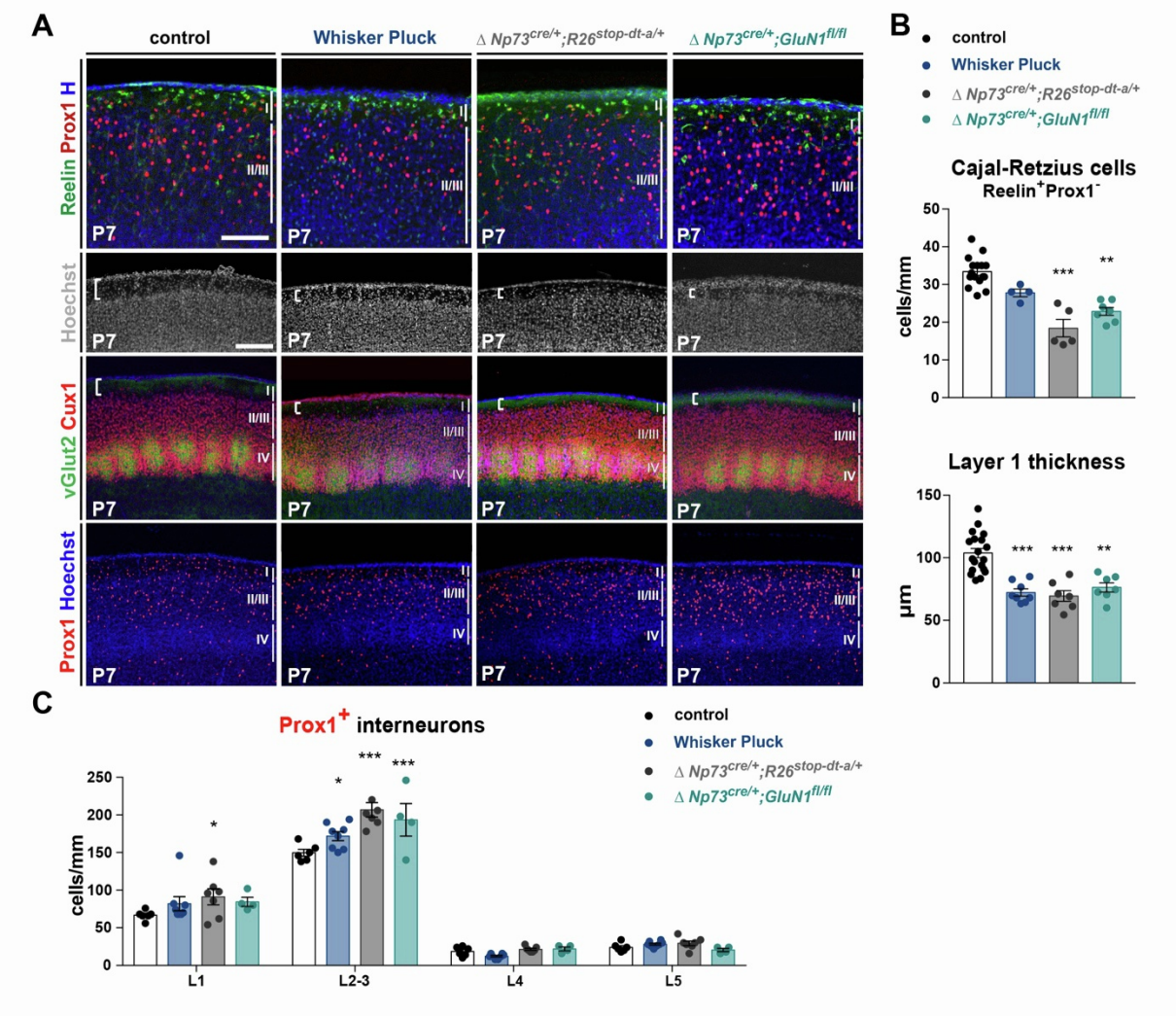

Figure S2, related to Figure 2. Sensory deprivation and decrease in Cajal-Retzius cell density alter L1 thickness and interneuron distribution in the first postnatal week.

(A) Confocal images of coronal sections in the barrel cortex (S1bf) of P7 controls, animals that were Whisker Plucked postnatally (WP), *ΔNp73*$^{cre/+}$*;R26*$^{dt\text{-}a/+}$ and *ΔNp73*$^{cre/+}$*;GluN1*$^{fl/fl}$ mutants. White brackets delineate L1. **(B)** Quantification of CRc numbers (in cells/mm of L1 length) identified as Reelin^{+}Prox1^{-} cells at P7 (n=16 for controls, n=4 for WP, n=5 for *ΔNp73*$^{cre/+}$*;R26*$^{dt\text{-}a/+}$ and n=7 for *ΔNp73*$^{cre/+}$*;GluN1*$^{fl/fl}$ mutants) and of L1 thickness (in µm) (n=19 for control, n=8 for WP, n=7 for *ΔNp73*$^{cre/+}$*;R26*$^{dt\text{-}a/+}$ mutants and n=7 for *ΔNp73*$^{cre/+}$*;GluN1*$^{fl/fl}$ mutants). **(C)** Quantification of Prox1^{+} interneuron distribution in each layer of the neocortex reveals an increase in all experimental conditions, compared to controls (n=5 for controls, n=8 for WP condition, n=7 for *ΔNp73*$^{cre/+}$*;R26*$^{dt\text{-}a/+}$ and n=4 for *ΔNp73*$^{cre/+}$*;GluN1*$^{fl/fl}$ mutants). Values are expressed as mean ± SEM, Kruskal-Wallis multiple comparison test in (B) and 2-ways ANOVA with Dunnett's multiple comparison correction in (C). * p<0.05; **p<0.001; ***p<0.0001. Scale bar represents 200 µm.

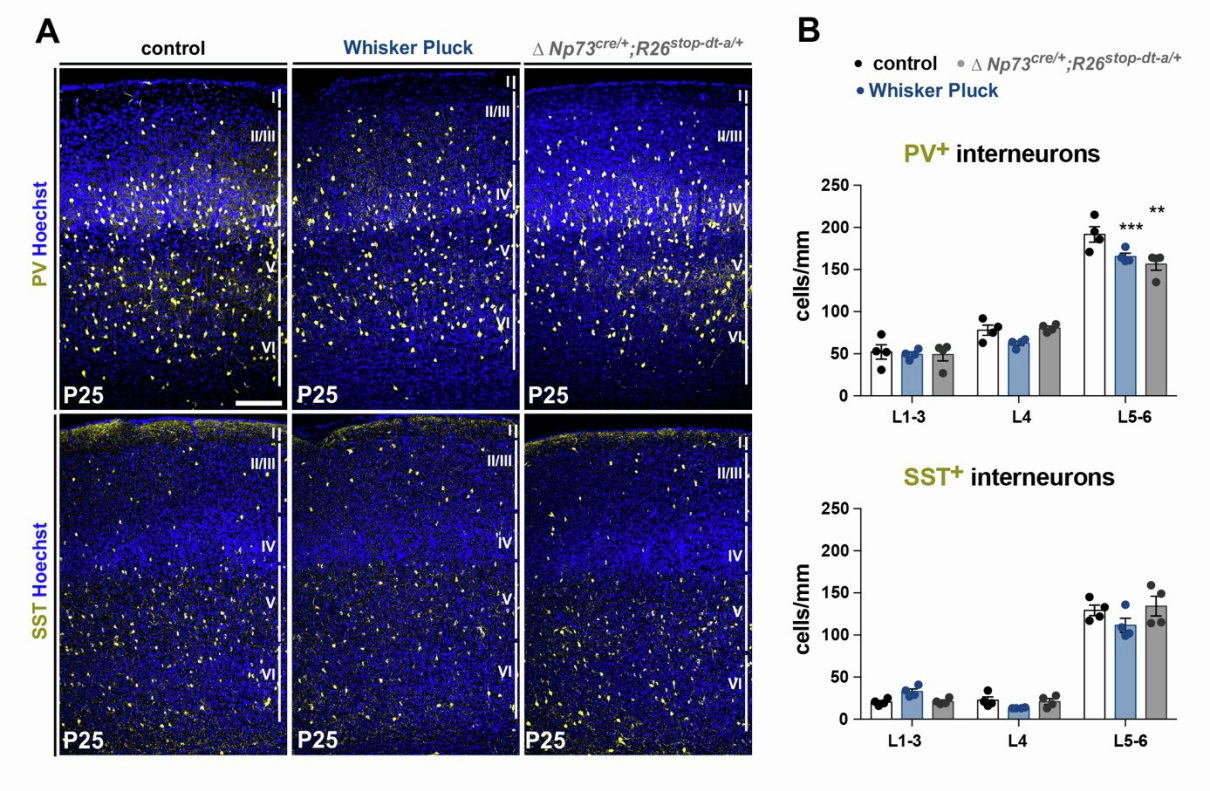

Figure S3, related to Figure 3. Sensory deprivation and a decrease in Cajal-Retzius cell density modify PV^{+} interneuron distribution.

(A) Confocal images of coronal sections in the barrel cortex (S1bf) of P25 controls, animals that were Whisker Plucked postnatally (WP) and *ΔNp73$^{cre/+}$;R26$^{dt\text{-}a/+}$* mutants showing PV and SST immunostainings, that mark two non-overlapping populations of MGE-derived interneurons. **(B)** Quantifications of MGE-derived interneuron density in upper cortical layers (L1-3), layer 4 and deep cortical layers (L5-6), showing a selective impact on the distribution of PV^{+} interneurons in both experimental models (n=4 for controls, n=4 for WP and n=4 for *ΔNp73$^{cre/+}$;R26$^{dt\text{-}a/+}$* mutants). Values are expressed as mean ± SEM, 2-ways ANOVA with Dunnett's multiple comparison correction, * p<0.05; **p<0.001; ***p<0.0001. Scale bar represents 200 µm.

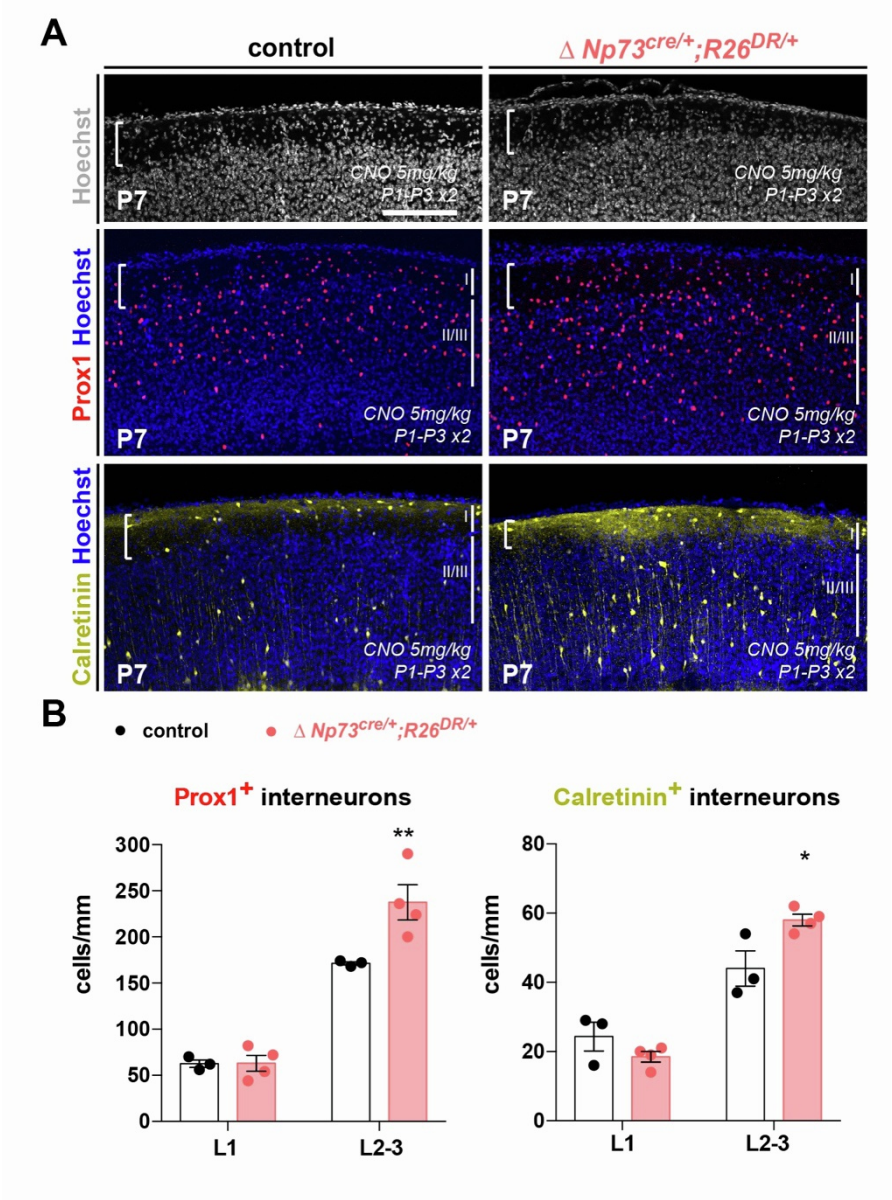

Figure S4, related to Figure 5. Reduction in both prenatal and postnatal CRc density perturb interneuron distribution at P7.

(A) Confocal images of coronal sections in the barrel cortex of P7 controls and *ΔNp73*$^{cre/+}$*;R26*$^{DR/+}$mutants, both having received CNO injections between P1 and P3. Immunostainings against Prox1 that labels all POA/CGE-derived interneurons and against Calretinin which labels a subpopulation called bipolar neurons. **(B)** Quantifications of Prox1^{+} and Calretinin^{+} interneuron densities in L1 and L2-3 in the barrel cortex of P7 controls and *ΔNp73*$^{cre/+}$*;R26*$^{DR/+}$mutants, showing an increase in interneuron numbers in both mutant backgrounds (Prox1: n=3 for controls and n=4 for *ΔNp73*$^{cre/+}$*;R26*$^{DR/+}$ mutants; Calretinin: n=3 for controls and n=4 for *ΔNp73*$^{cre/+}$*;R26*$^{DR/+}$ mutants). Values are expressed as mean ± SEM, 2-ways ANOVA with Sidak's multiple comparison correction in (B), * p<0.05; **p<0.001; ***p<0.0001. Scale bar represents 200 µm.